

The impact of changing lightning step leader position on the performance of LPS (lightning protection system) for wind turbines

Younes Abdelbari¹, Mimouni Abdenbi¹

¹Laboratory of Electrical Engineering and Plasmas

Univ. Ibn khaldoun, Tiaret, Algeria

Email : abdenbi.mimouni@gmail.com

Abstract - If the receivers on the wind turbine blade do not manage to block the lightning, the blade or the wind turbine (WT) may be destroyed. So the receiver plays a key part in identifying the lightning protection (LSP) system on WT. In this paper, we applied three types of tip receivers with various dimensions and forms to a classic wind turbine blade and various positions of the lightning step leader to examine their role in the LSP. A computer model using finite element analysis (FEA) has been used to predict the electrostatic field at the blade area as a result of a lightning strike. The effectiveness of the interception is assessed by making a comparison between the maximal expected electric field intensity in the proximity of the receivers in one of the two blade faces. The highest electric field intensity in trailing and leading compared to distance from the root where it was noticed that there is an impact of the changing lightning position on the performance of (LSP). Furthermore, the location of the lightning fixation points with the WT blade matches well with the one obtained from actual experiments, which supports the numerical design.

Keywords - Lightning, wind turbines, Load.

I. INTRODUCTION

Over the last decade, the total number of wind farms has increased significantly, and the energy generated by wind has developed into one of the main renewable energy options [1] with a full potential of over 970.2GW and 21987 wind farms by the end of 2020 [2].

As a result of the high energy production and the demand for better wind conditions, wind turbines are becoming taller, the swept area is getting larger and they are also moving offshore, which puts them at greater risk of lightning strikes [3]. Lightning damage can often be costly to repair and can cause serious downtime. As an example, about 85% of all shutdown times associated with the start-up of commercial wind farms in the south-western United States were due to lightning and the full cost related to lightning surpassed \$250,000. In some cases, the increase in the dimensions of wind turbines over the past few years presents significant obstacles to the design of lightning protection systems (LSP) [4].

The LSP approach most frequently used is the integration of receivers in the area of the blades wind turbines. These receivers are attached to a down conductor within the blade, extending down the base to the point of the blade. They are made to catch lightning strikes and conducts the lightning current safely across the descending wires to ground. The performance of the LSP is stated as the combination of the performance of the interception and the performance of the current sizing. In which the intercept capability is the capacity of capture a lightning strike and the current sizing efficiency is the capacity to drive the lightning current of the LSP equipment [5], the effectiveness of the dimensioning may be augmented by making the down conductors larger in diameter. Nevertheless, the interception performance is highly based on the geometry and site of the receivers and requires further study. While a receiver on both sides of the tip blade is supposed to be a good LSP solution for the under 20 m blades [5]. As a result of the practical absence of evaluating

interception performance. So far, few experiments have been done to investigate the impact of receiver geometry on reception in Arif and al [6], Guo and al [7], Li and al [8]. In that respect, related simulation research has been rarely reported. In order to find options for evaluating the success of the interception, a forecasting model is recommended in this document and is used in the design and dimensioning receiver [4].

This document applies receptors of various forms to the area of the blade wind turbine and changes the positions of the lightning step leader. A computed model with finite element analysis (FEA) has been set up to obtain the electric field intensity at the blade area of the wind turbine because of a lightning tracer. The anticipated position of the lightning strike connection spot on the blade area is referred to be the site of maximum electric field strength magnitude. In order to evaluate the receptor's interception performance, the associated maximum strengths of the electric field on receivers of various settings are compared [4].

II. DEFINITION OF THE PROBLEM

A) Lightning Stepped Driver Model

In this article, we concentrate on the study of lightning downwash interaction with wind turbine blades. A representative lightning downward that begins with weak lightning leaves the cloud and travels through the air into the soil structure. The response pulses are transmitted by ground-based level structures if the gradient of the electric field from the lightning tracer tip to the floor-based structure is adequate to break up the air between them. If a response pulse is emitted by the ground structure, it stops the lightning rod. Then the primary lightning flashback is generated [9].

The lightning step leadership model suggested by Cooray and al [10] has been employed in [11] and [12] for the estimation of lightning-induced electric fields. In the design, the leader of lightning steps is idealised as follows: an upright line load with non-uniform load density:

$$\lambda(\eta) = a_0 \left(1 - \frac{\eta}{H - z_0} \right) \cdot G(z_0) \cdot I_{\text{peak}} + \frac{I_{\text{peak}} \cdot (a + b \cdot \eta)}{1 + c \cdot \eta + d \cdot \eta^2} \cdot F(z_0) \quad (1)$$

$0 \leq \eta \leq L, z_0 \geq 10, G(z_0) = 1 - (z_0 / H), F(z_0) = 0,3\alpha + 0,7\beta, \eta = z - z_0, \beta = 1 - (z_0 / H), \alpha = \exp(-(z_0 - 10) / 75),$ with $a_0 = 1,476 \cdot 10^{-5}, a = 4,857 \cdot 10^{-5}, b = 3,9097 \cdot 10^{-6}, c = 0,522, \text{ et } d = 3,73 \cdot 10^{-3}.$

Where $\lambda(\eta)$ is the charge density (in C/m); η (in m) is the distance; H is the cloud height to the ground (usually $H = 4000$ m); z_0 stands for the range of soil to the leader's tip (m); I_{peak} is the current peak of the feedback stroke (in kA). The load density determined with (1) indicates a favourable consensus with the physical dimensions as referred by Cooray and al [10]. Therefore, the lightning tiered leader format (1) including the same data as above is applying in this document. The basic uniform electric field from the sky to the earth would be 10 kV/m [13], and the distance of the cloud to the earth is usually considered as 4000 m [14] and [12], this is why, the voltage $V = 40$ MV [13], is used here. The earth is a map with zero electrical potential.

B) Geometry Wind Turbine and Setup

The national laboratory for renewable energy (NREL) 5 MW wind turbine design [15] is employed for the development of a design for the impact analysis of lightning. The parts geometries of the turbine are modelled using the measurements of the NREL standard turbine (Fig. 1).

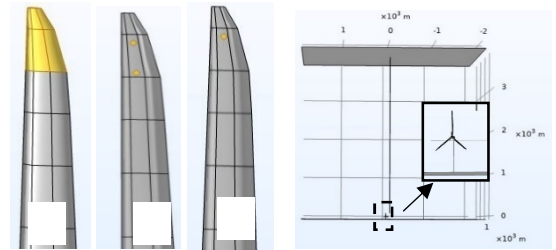


Fig. 1. Three various receiver settings used in the simulation study and COMSOL Multiphysics Problem setup

Table 1. Three various receiver configurations.

Configurations	Receptor Characteristics
Configuration 1	Receiver tip, with a length of 4 m (tip extension)
Configuration 2	Double receiver in the shape of a small disc, radius 0.2 m, gap from the tip to the first receiver 1.92 m, and between the two receivers 1.92 m
Configuration 3	receptor in the form of a small disc, distance from the tip 1.92 m, radius 0.2 m

The most precise lightning-induced electric fields are produced by accurate blade design rather than by

employing a simplified design [16]. In our document, the blade length, hub radius and hub height are 60, 1.5 and 90 metres respectively [17], [18]. So, the peak height of the blade tip with one blade in the upper vertical emplacement is 151.5 m.

To study the impact of the receivers, three various combinations of receivers (Figure 1) are being applied to the wind turbine blades. Configurations use receivers in various shapes (disc and tip form) and dimensions (radii/ lengths) on the blade tip as shown in table I. All receivers in configurations 1 to 3 are attached to the exact same descent conductor in the blade body section. The configurations are selected because tip and disc receptors are the best commonly used on current blades of wind turbines and a large number of disc receptors are also extensively employed on blades over 20 m [5].

In any case presented in this document, the blades of the turbine are positioned on the tower, with one blade in the upper standing position. The impact of the dynamic rotation of the blades is not taken into account in this research. The lightning strike distance from the stepped leader to the wind turbine was computed by the rolling sphere approach [19], [10] and [20].

$$R = 0.6 \cdot I_{\text{peak}}^{1.46} \quad (2)$$

R is the lightning strike length (in m) and I_{peak} is the maximum peak current (in kA). As recommended by [5], it is suitable to apply the rolling sphere approach to the present current model of wind turbine with blades of greater length than 20 m. Moreover, the rolling sphere is supposed to be tangential to the tip top blade positioned.

The top 50% of the recorded negative return strokes have a maximum peak current of 30 kA, following to Gameraota and al [21]. Thus, in this paper, the maximum current I_{peak} that is applied in every simulation is chosen to be 30 kA to show the global lightning strike situation.

III. NUMERICAL IMPLEMENTATION

The approximated electric fields for the wind turbine blades of various receiving in the presence of lightning strikes are determined by FEA. The equations governing the issue, as well as the related

numerical configuration and application are examined in this part.

A) Governing Equations

The electrostatic equations can be used to calculate the electric field produced by a vertically loaded lightning stepped leader.

$$\nabla \times \mathbf{E} = 0, \quad (3)$$

$$\nabla \cdot \mathbf{E} = \frac{\rho_v}{\epsilon_0}, \quad (4)$$

$$\mathbf{E} = -\nabla\phi \quad (5)$$

Here E stands for the electric field density, ρ_v is the origin of electric charge $\rho_v = \lambda/\pi r^2$, λ is the lineal charge density (1), r is the radius of the cylindrical vertical lightning rod channel, $r = 1.5$ m, ϵ_0 the permittivity of open area, and ϕ the electric potential.

The lightning strike range (2) defines the relative area location of the lightning strike and the geometry of the wind turbine in the calculation sector, also sets out the positions of the zero electrical potential border conditions which are related to lightning energy.

B) Numerical Method

To get the governance (3)-(5) solved, the FEA COMSOL Multiphysics software is used. As shown in Figure 2, the calculation domain range is $4000 \text{ m} \times 4000 \text{ m} \times 4000 \text{ m}$ using a cut-out of the proposed wind turbine design. How situated on the grounds. Lightning strike driver in the middle of the sector and extends from the surface area over 151,5 m over floor level. The (2) determines the lightning's range to the wind turbine. We changed the locations of the wind turbines according to the lightning strike as indicated in Figure 2.

In the ensemble of the calculation area, the four lateral surfaces are implemented with an open boundary requirement. Moreover, the hub, nacelle and tower areas of the wind turbine configuration are applied at a mass potential, for the reason that the materials employed in these parts are generally steel and aluminium [22], which are electrically conducting. To keep in mind, the impact of the receivers, a ground potential is additionally imposed on the areas of the tip receiver employed in configuration 1 and the disc receptors employed in configurations 2 and 3. The rest of the wind turbine blade surface is under open limit requirements as the

rest of the blade surface is made up of electrically non-conductive materials (laminated glass fibre composite fabrics).

The calculation sector and the lightning leader are allocated to an "air" material as specified in the COMSOL material reference library. The upper part of the domain surface is imposed with a voltage cloud $V = 40$ MV [13], the calculation domain has meshed with 2,216,139 (the average number of all case simulations) free tetrahedral elements more than [4], the maximum and minimum values of the components are 250 and 0.017 m respectively.

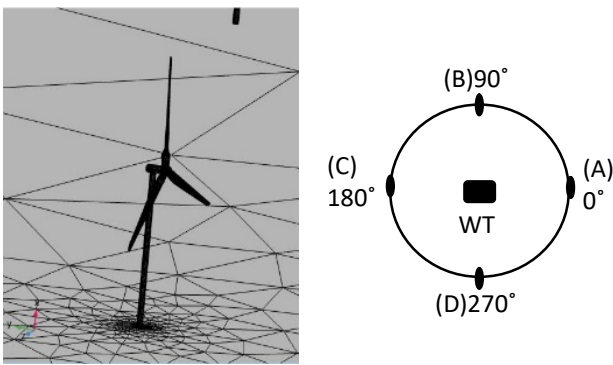


Fig. 2. Area mesh related to the high precision model of the wind turbine.

The maximum growth rate of the elements is 1.5, and the regulation of the curvature and narrow areas is 0.5 and 0.6 respectively. In seeking to ensure a balance between performance and computational precision, the meshes near the turbine are refined. An illustration of the area mesh related to the wind turbine is presented in Figure 2. While it seems that the highest size of the element, 250 m, is adequately large to obtain an exact distribution of the electric field.

Our study (see section IV) indicates that the highest element size of 250 m is sufficiently low for the present simulation work. At the same time, the reduction of the maximum size of the elements will cause a major rise in the number of elements, thus calling for large calculation memory. Within our current computing capacity, with a quad-core laptop and 8 GB of RAM, we tested that 250 m was the lowest maximum value of the simulation elements to be successfully executed. If a bigger workstation is used, a much finer mesh may be applied to obtain a much higher precision.

IV. RESULTS AND DISCUSSIONS

This part sets out the expected electric field intensities at the slide surfaces using three receiver configurations. It is important to take note that just the findings for the upper part of the vertical blade are examined in this article since the related electric fields are significantly higher than on the zones of the remaining two blades. The positions of the highest electric fields on the surface zone of the blades allow us to provide a great possibility to issue respondent leaders and to stop the flash leader.

Firstly, the electric field intensity associated with the largest element dimension is illustrated. Figure 3 presents the differences in the expected electric field spread in the blade tip zone which was achieved in the model, which was set to 550m-Figure 3(a), 450m-Figure 3(b), 350m-Figure 3(c) and 250m- Figure 3(d), respectively. As illustrated in figure 3, the maximum electric fields produced with the four various maximum element sizes have the same magnitude, but employing a large mesh dimension of 250 m gives the most consistent method of electric field estimation. Consequently, to obtain a preserver expectation, a maximum element dimension of 250 m is applied to all the calculation findings in the subsequent paper.

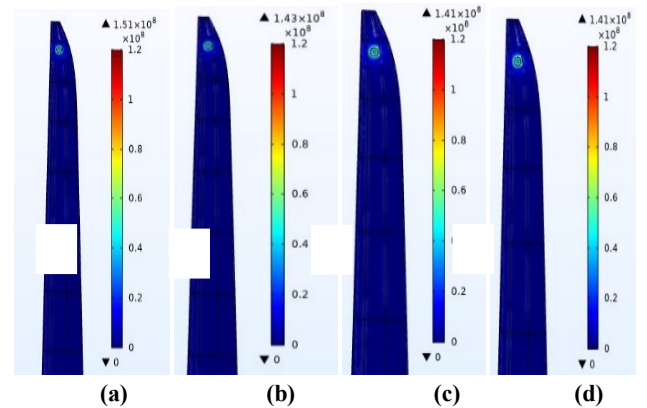


Fig. 3. Effects of highest mesh size on the expected distributions of electric field strength in the tip areas : (a) highest mesh size equals 550 m; (b) highest mesh size equals 450 m; (c) highest mesh size equals 350 m; and (d) highest mesh size equals 250 m.

Fig. 4, 5 and 6 has the greatest electric field intensity in the region of the total tip zone can be determined by drawing the electric field intensity distributions for the three various receptor settings in different positions of wind turbine.

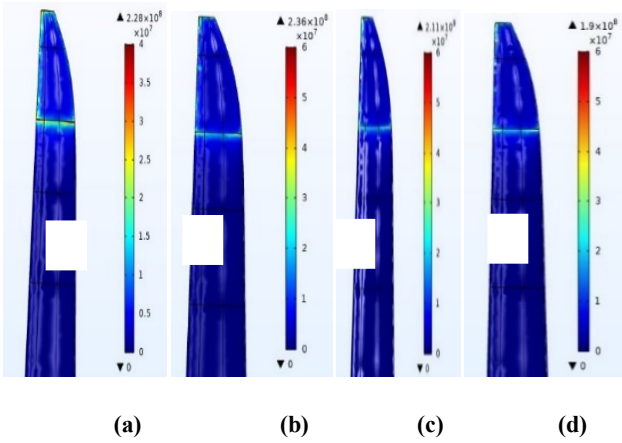


Fig. 4. Comparison of expected electric field intensity distributions at the tip regions for different positions (Configuration 1): (a) position A; (b) position B, (c) position C, (d) position D.

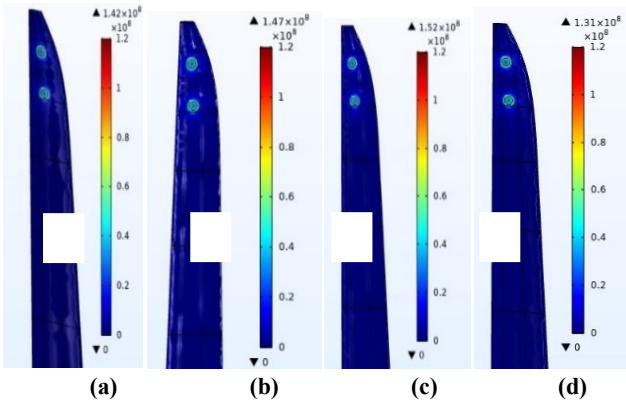


Fig. 5. Comparison of expected electric field intensity distributions at the tip regions for different positions (Configuration 2): (a) position A; (b) position B, (c) position C, (d) position D.

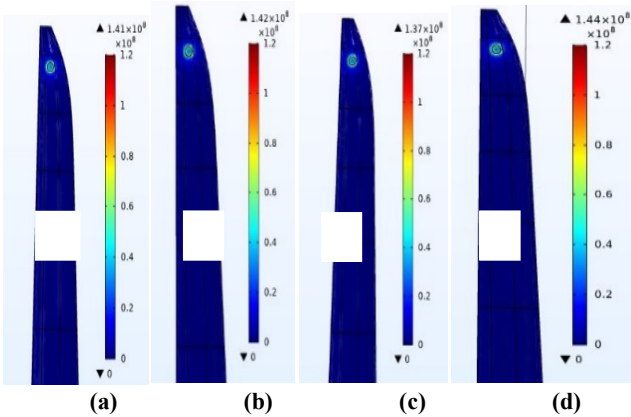


Fig. 6. Comparison of expected electric field intensity distributions at the tip regions for various positions (Configuration 3): (a) position A; (b) position B, (c) position C, (d) position D.

Table 2. Maximum expected electric field intensity

10^8 v/m	A	B	C	D
tip	2.28	2.36	2.11	1.9
Dual small disc	1.42	1.47	1.52	1.31
small disc	1,41	1,42	1,37	1,44

It is possible to see there is a difference in top electrical field strength in different positions for the identical type of receptor from table II. For tip-shaped (configuration 1) receptor has the maximum electric field as in position B with 3.38 % higher than second-greatest electric field (position A), the lowest electric field as in position D with 11.05% lower than second-lowest electric field (position C). But for dual small disc receiver (configuration 2) has the maximum electric field as in position C with 3.28 % more than second-greatest electric field (position B), the lowest electric field as in position D with 8.39% lower than second-lowest electric field (position A). last for small disc receiver has the maximum electric field as in position D with 1.38 % more than the second-greatest electric field (position B), the lowest electric field as in position C with 2.38% lower than the second-lowest electric field (position A).

To fully understand these variations, the electric field intensity of the wind turbine blade following the leading and trailing sides of the three configurations as shown. In this article, there are no plots to illustrate the electric field intensity comparison across a range of 0 to 55 m from the root of the trailing side for the four various positions with the three receiver configurations 1, 2 and 3. where their electric field intensity for various positions with three configurations are similar within 0-50 m from the root. Figure 7 indicates the forecast field corresponding to the electric field intensity across the trailing side of the tip areas (55-60 m from the root) of the blade designs with tip form receivers. It shows that the electric field intensity in the zone of the tip is much more than two orders of magnitude more than that at the in-edge area for the situations where receivers are in place. We can find in figure 7 that the electric field intensity for various positions with configuration 1 is almost identical except for a various peak value in 57.52m of the root. The biggest peak electric field as in position A with 223.02Mv/m than second-highest electric field (position B) with

214.75Mv/m, the lowest electric field as in position D with 188.41Mv/m than second-lowest electric field (position C) 207.17Mv/m.

Fig. 8 indicate the expected field intensity associated with the electric field intensity across the trailing edge of the tip zones at 55-60 m from the blade root of the blade designs with Dual small disc form receivers. The figures show that this four identical curves but one on top of the other, including two peak one at 57.90m from root and secondary at 60.11m from root. the greatest peak electric field as in position A with 3.47Mv/m than second greatest electric field (position B) with 3.38Mv/m, the lowest electric field as in position D with 3.37Mv/m than second lowest electric field (position C) 3.28Mv/m. lastly figure 9 shows the expected the electric field intensity across the

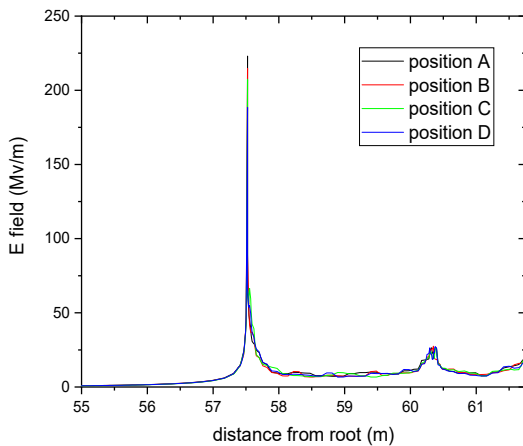


Fig. 7. Comparison of expected electric field along the trailing edge in the range of 55-61.5 m from the root for various positions settings.

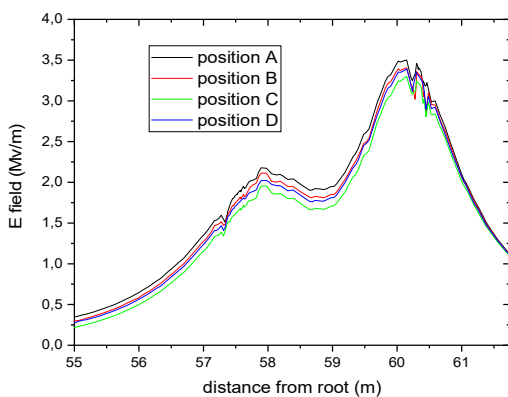


Fig. 8. Comparison of expected electric field intensity along the trailing edge in the 55-61.5 m from the root for various positions

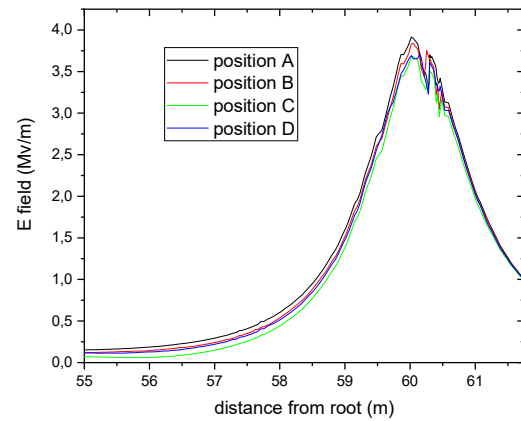


Fig. 9. Comparison of expected electric field along the trailing edge in the range of 55-61.5 m from the root for various positions settings.

trailing edge at 55-60 m from the blade root of the blade designs with small disc shape receptors. The figures show that this four identical curves but one on top of the other, including one peak at 60m from root. the highest peak electric field as in position A with 3.91Mv/m than second greatest electric field (position B) with 3.83Mv/m, the lowest electric field as in position D with 3.69Mv/m than second lowest (position C) 3.65Mv/m.

There are no plots to illustrate the electric field intensity comparison across a range of 0 to 55 m from the root of the leading edge for the four different positions with the three receiver configurations 1 to 3. The expected field intensity associated with the electric field intensity across the leading side of the tip zones at 55-60 m from the blade root of the blade designs with tip shape receivers is presented in figure 10. It may be seen that the electric field intensity in the peak area is higher where receivers are positioned. It can be observed in figure 10 that the electric field intensity for various positions with configuration 1 is almost identical except for two different peaks the first value in 57.42m and second in 61.5 m from the root. The highest peak electric field as in position A with 108.05Mv/m at the first peak. Than second highest electric field (position D) with 101.17Mv/m, the lowest electric field as in position C with 94.07Mv/m and second-lowest electric field (position A) 90.65Mv/m in the second peak.

Furthermore, in fig. 11, the relevant expected field intensity is associated with the electric field

intensity across the leading edge of the tip zones at 55-60 m from the blade root of the blade designs with double small disc receivers. From the figures we can see that these four positions curves are the same but include two peaks, the edge region the first at 57.60 m from the root and the second at 59.61m from the root. In position C the highest electric field was 6.52 Mv/m, in position B the second-highest electric field was 6.42 Mv/m, in position D the lowest electric field was 6.25 Mv/m and in position A, the second-lowest electric field was 5.84 Mv/m. Last, in fig. 12, the associated electric field is expected to have the electric field intensity across the leading edge at 55-60 m from the blade root of the blade designs with small disc receivers. From the figures we can see that these four positions curves are identical but include one peak, the edge region the first at 59.61m from the root. In position B the highest electric field was 5.9 Mv/m, in position C the second-highest electric field was 5.58 Mv/m, in position A, the lowest electric field was 5.55 Mv/m and

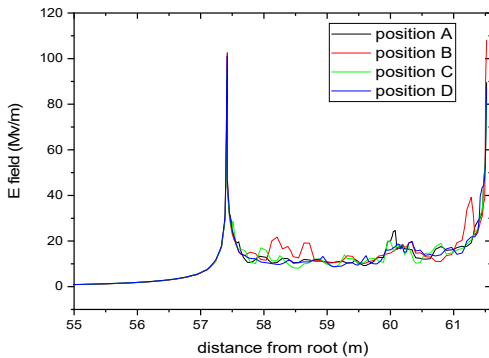


Fig. 10. Comparison of expected electric field intensity along the leading edge in the 55-61.5 m from the root for various positions.

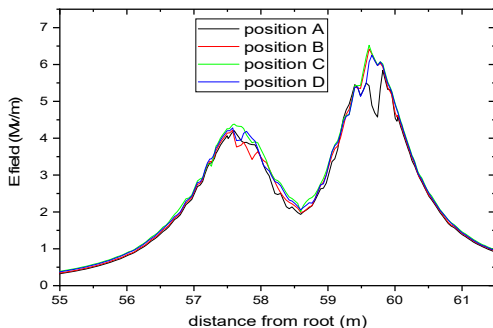


Fig. 11. Comparison of expected electric field along the leading edge in the 55-61.5 m from the root for various positions settings.

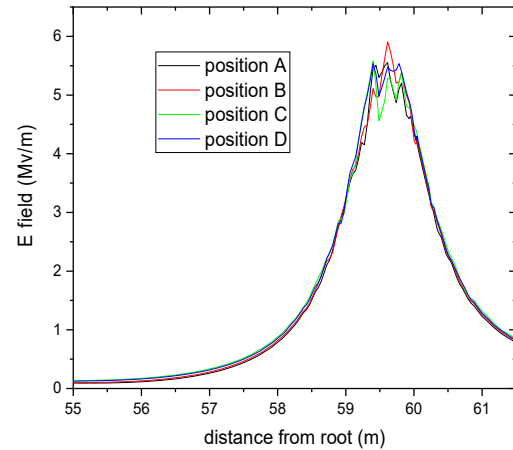


Fig. 12. Comparison of expected electric field along the leading edge in the 55-61.5 m from the root for various positions settings.

in position D, the second-lowest electric field was 5.53 Mv/m. These findings show that these receivers significantly improve the electric field intercepting. Therefore, responses to leaders are so much apt to be emitted from such receptors better than from the zone isolated. In this manner, the lightning current is passed through the receiver conductor and internal downward conductor without generating significant lightning damage to the isolated regions of the blades, the point of attachment the lightning to the area of a blade is selected where the amplitude of the electric field is the highest.

These findings show the electric field intensity at both edges is considerably higher when applying the tip receiver than when using the disc. This is due to the fact that the trailing and leading sides of blade employing discs are always nonconductive, while the trailing and the leading sides of blade models using the tip-shaped receivers are electrically driven. However, expanding the dimension of the receiver and increasing the receiver discs' number would negatively increase the blade's weight, which could raise the cost and may also affect the mechanical efficiency. The thin wire receiver may be an alternative. In addition, the position of the lightning step leader affected the efficiency of the reception.

V. CONCLUSION

In this paper, the potential impact of LSP receivers on wind turbines was examined with various positions of the lightning step leader. The varying

charge density of the lightning tracer was included in the computer system. The capture performance for the receivers with various positional configurations was determined by matching the expected maximum electrical power and the field intensity on the blade area.

Our findings show that the tip spike receptor performs significantly better in interceptions than the disc receiver in various positions of the lightning step leader. The direction in which a descending lightning tracer approaches is found to be a very significant factor in the interception performance of a wind turbine's lightning protection system. In general, the growth in the size of the receiver and the rise the number of discs can equally rise the interception performance. Nevertheless, the extra weight might lead to increased costs and a risk of compromise in mechanical capacity.

It is significant that the findings of this present computer model will inevitably be influenced by the lightning range design adopted and the specification of stimulus settings such as minimum and maximum mesh size and growth factor of the elements. The approach presented here can be used to assess the effectiveness of interception by receptors to improve the design and construction of sophisticated lightning receivers by optimising configurations.

The study of several types of receivers with various positions of the WT and split analysis was able to catch electric field diffusion within the structure of the blade or the mechanical effect of the receiver on the blades, something that will be the topic of our next research.

VI. REFERENCES

- [1] V. Peesapati, I. Cotton, T. Soerensen, T. Krogh, and N. Kokkinos, "Lightning protection of wind turbines—A comparison of measured data with required protection levels," *Renewable Power Generation, IET*, vol. 5, pp. 48–57, Feb. 2011, doi: 10.1049/iet-rpg.2008.0107.
- [2] "Wind energy database," 2020. <https://www.thewindpower.net/index.php>.
- [3] G. Ikhazuangbe, M. Begam, C. Gomes, S. Shanmugam, and K. Nwizege, "Optimum Receptor Location for Efficient Lightning Protection of Modern Wind Turbines," *International Journal of Simulation: Systems, Science & Technology*, vol. 18, Sep. 2017, doi: 10.5013/IJSSST.a.18.03.04.
- [4] Y. Wang and W. Hu, "Investigation of the Effects of Receptors on the Lightning Strike Protection of Wind Turbine Blades," *IEEE Transactions on Electromagnetic Compatibility*, vol. 59, no. 4, pp. 1180–1187, Aug. 2017, doi: 10.1109/TEM.2016.2647260.
- [5] International Electrotechnical Commission, *Wind turbines. Part 24, Part 24.* Geneva: International Electrotechnical Commission, 2010.
- [6] W. Arif, Q. Li, Z. Guo, M. Aizaz, Y. Ma, and W. H. Siew, *Experimental Study on Interception Failure of Lightning Protection System of Wind Turbine Blade*. 2017. doi: 10.1109/ICET.2017.8281723.
- [7] Z. Guo, Q. Li, W. Yu, W. Arif, Y. Ma, and W. H. Siew, "Experimental Study on Lightning Attachment Manner to Rotation Wind Turbine Blade," in *2018 34th International Conference on Lightning Protection (ICLP)*, Sep. 2018, pp. 1–5. doi: 10.1109/ICLP.2018.8503300.
- [8] X. Li, J. Guo, X. Chen, K. Yang, T. He, and X. Wang, "Experimental and Numerical Analysis of the Effect of a New Lightning Protection System on Lightning Protection and Aerodynamic Noise Performance of Wind Turbine Blades," *Electronics*, vol. 8, no. 9, Art. no. 9, Sep. 2019, doi: 10.3390/electronics8091020.
- [9] V. A. Rakov and M. A. Uman, *Lightning: Physics and Effects*. Cambridge University Press, 2003.
- [10] V. Cooray, V. Rakov, and N. Theethayi, "The lightning striking distance—Revisited," *Journal of Electrostatics*, vol. 65, no. 5, pp. 296–306, May 2007, doi: 10.1016/j.elstat.2006.09.008.
- [11] J. R. Hermoso, J. Montanyà, V. March, D. Romero, G. Solà, and O. van der Velde, "A propagative model for simulations of electric fields produced by downward leaders," in *2010 30th International Conference on Lightning Protection (ICLP)*, Sep. 2010, pp. 1–4. doi: 10.1109/ICLP.2010.7845947.
- [12] A. BAKAR *et al.*, "Determination of the striking distance of a lightning rod using finite element analysis," *TURKISH JOURNAL OF ELECTRICAL ENGINEERING & COMPUTER SCIENCES*, vol. 24, pp. 4083–4097, Jan. 2016, doi: 10.3906/elk-1311-175.
- [13] M. Becerra, "On the Attachment of Lightning Flashes to Grounded Structures," 2008, Accessed: Jul. 16, 2021. [Online]. Available: <http://urn.kb.se/resolve?urn=urn:nbn:se:uu:diva-8871>
- [14] V. Cooray, M. Becerra, and V. Rakov, "On the electric field at the tip of dart leaders in lightning flashes," *Journal of Atmospheric and Solar-Terrestrial Physics*, vol. 71, no. 12, pp. 1397–1404, Aug. 2009, doi: 10.1016/j.jastp.2009.06.002.
- [15] J. Jonkman, S. Butterfield, W. Musial, and G. Scott, "Definition of a 5-MW Reference Wind Turbine for Offshore System Development," National Renewable Energy Lab. (NREL), Golden, CO (United States), NREL/TP-500-38060, Feb. 2009. doi: 10.2172/947422.

- [16] Y. Wang and O. Zhupanska, "Estimation of the electric fields and dielectric breakdown in non-conductive wind turbine blades subjected to a lightning stepped leader," *Wind Energy*, vol. 20, pp. 927–942, Nov. 2016, doi: 10.1002/we.2071.
- [17] W. Hu, K. K. Choi, O. Zhupanska, and J. H. J. Buchholz, "Integrating variable wind load, aerodynamic, and structural analyses towards accurate fatigue life prediction in composite wind turbine blades," *Struct. Multidiscip. Optim.*, vol. 53, no. 3, pp. 375–394, Mar. 2016, doi: 10.1007/s00158-015-1338-5.
- [18] W. Hu, K. K. Choi, and H. Cho, "Reliability-based design optimization of wind turbine blades for fatigue life under dynamic wind load uncertainty," *Struct Multidisc Optim*, vol. 54, no. 4, pp. 953–970, Oct. 2016, doi: 10.1007/s00158-016-1462-x.
- [19] V. A. Rakov, "The Physics of Lightning," *Surv Geophys*, vol. 34, no. 6, pp. 701–729, Nov. 2013, doi: 10.1007/s10712-013-9230-6.
- [20] Y. Xu and M. Chen, "Striking distance calculation for flat ground and lightning rod by a 3D self-organized Leader Propagation Model," in *2012 International Conference on Lightning Protection (ICLP)*, Sep. 2012, pp. 1–5. doi: 10.1109/ICLP.2012.6344261.
- [21] W. R. Gamerota, J. O. Elismé, M. A. Uman, and V. A. Rakov, "Current Waveforms for Lightning Simulation," *IEEE Transactions on Electromagnetic Compatibility*, vol. 54, no. 4, pp. 880–888, Aug. 2012, doi: 10.1109/TEMC.2011.2176131.
- [22] D. Ancona and J. McVeigh, "Wind turbine-materials and manufacturing fact sheet," *Princeton Energy Resources International, LLC*, vol. 19, 2001.